Supporting Information

Nonlinear Optical Chromophores with Two Ferrocenyl, Octamethylferrocenyl, or 4-(Diphenylamino)phenyl Groups attached to Rhenium(I) or Zinc(II) Centers

Benjamin J. Coe,[†] Simon P. Foxon,[†] Rachel A. Pilkington,[†] Sergio Sánchez,[†] Daniel Whittaker,[†,‡] Koen Clays,[§] Griet Depotter,[§] and Bruce S. Brunschwig[⁋]

[†] *School of Chemistry, University of Manchester, Oxford Road, Manchester M13 9PL, U.K.*

[‡] *Current address: National Nuclear Laboratory, Sellafield, Seascale, Cumbria CA20 1PG, U.K.*

[§] *Department of Chemistry, University of Leuven, Celestijnenlaan 200D, B-3001 Leuven, Belgium*

[⁋] *Molecular Materials Research Center, Beckman Institute, MC 139-74, California Institute of Technology, 1200 East California Boulevard, Pasadena, California 91125*

1. Additional Electrochemical, Crystallographic and Spectroscopic Figures/Data

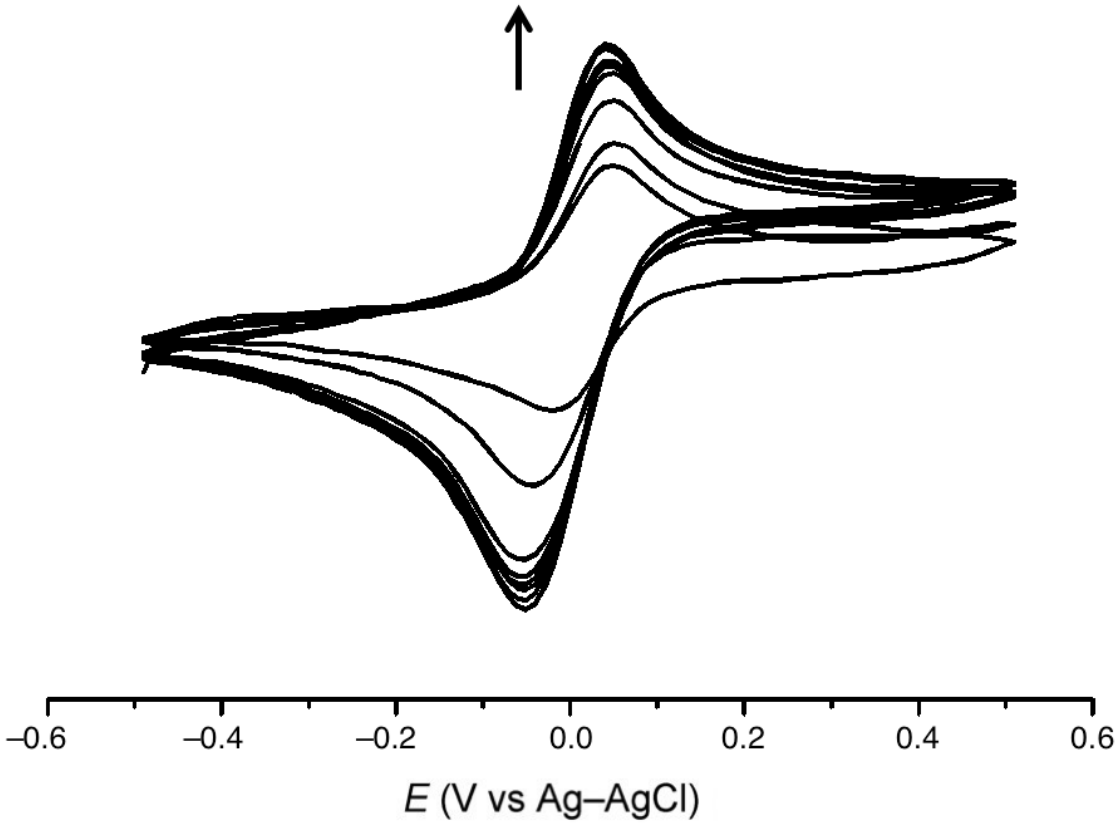

Figure S1. Cyclic voltammograms of $(Me_8Fcv)_2bpy$ recorded at 100 mV s^{-1} in DCM (0.1 M in $[N(C_4H_9\text{-}n)_4]PF_6$) with a glassy-carbon working electrode. The single-headed arrow indicates the increase in current with repeated cycles, due to the deposition of an electroactive film.

(a)

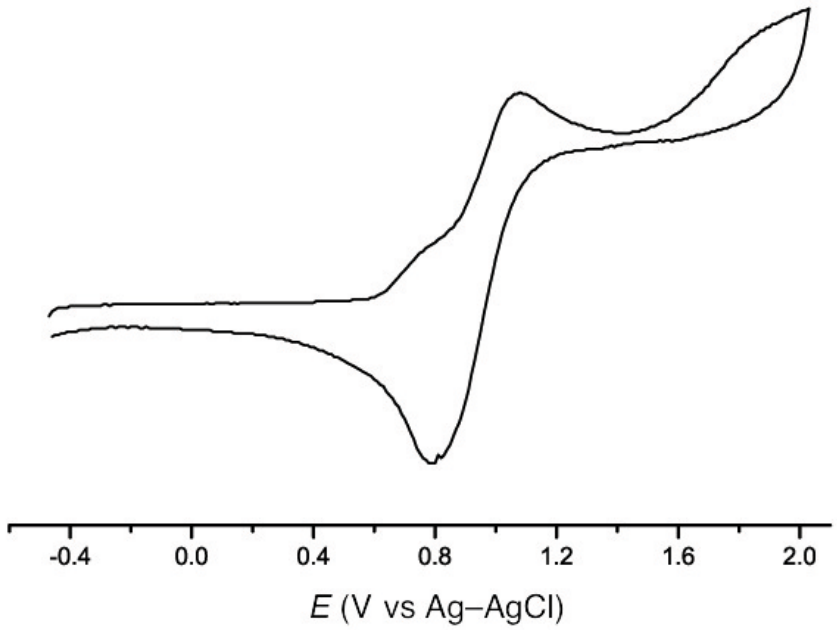

(b)

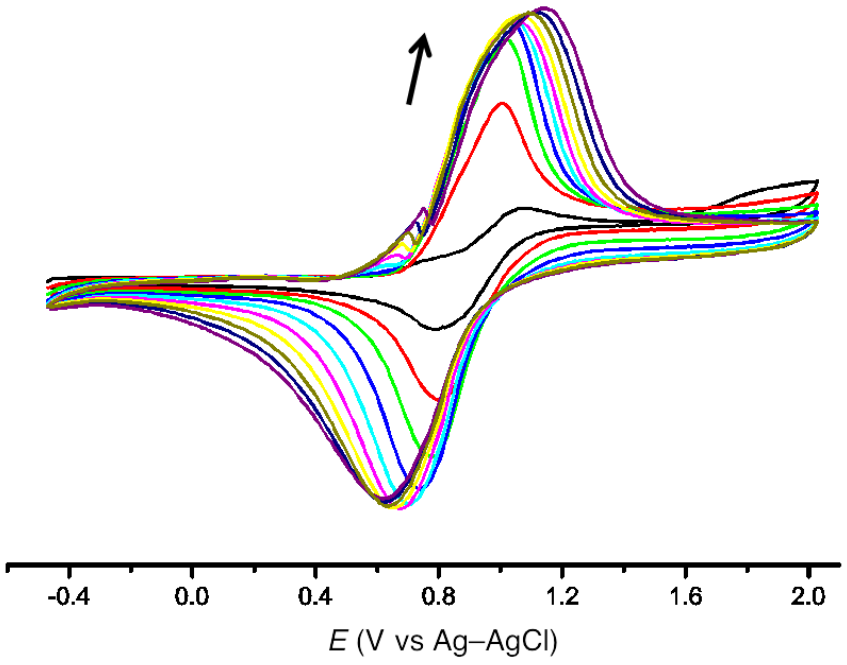

Figure S2. Cyclic voltammograms of $(Dapv)_2bpy$ recorded at 100 mV s^{-1} in DCM (0.1 M in $[N(C_4H_9\text{-}n)_4]PF_6$) with a glassy-carbon working electrode; (a) first cycle; (b) repeated cycles, with the single-headed arrow indicating the increase in current due to the deposition of an electroactive film.

(a)

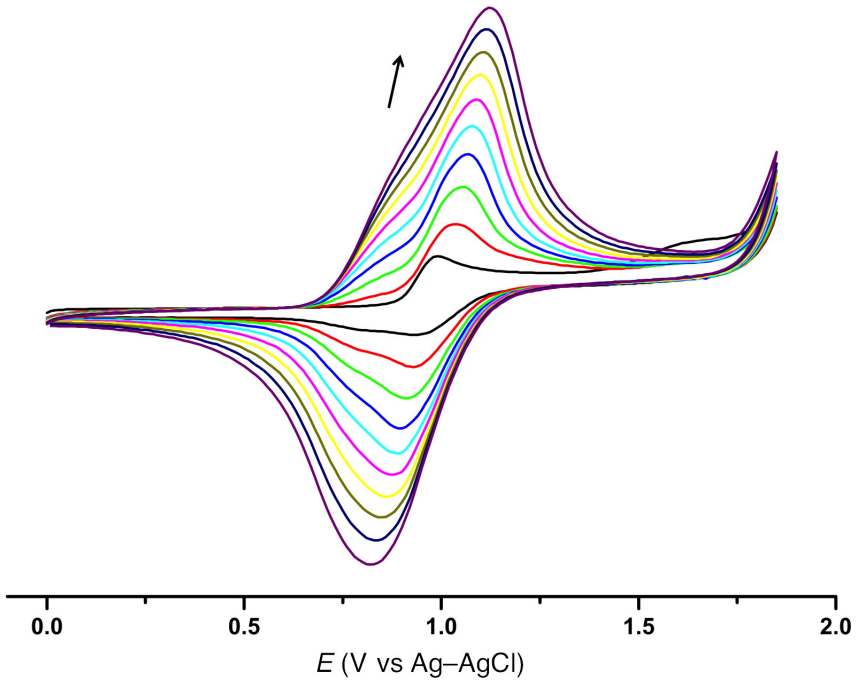

(b)

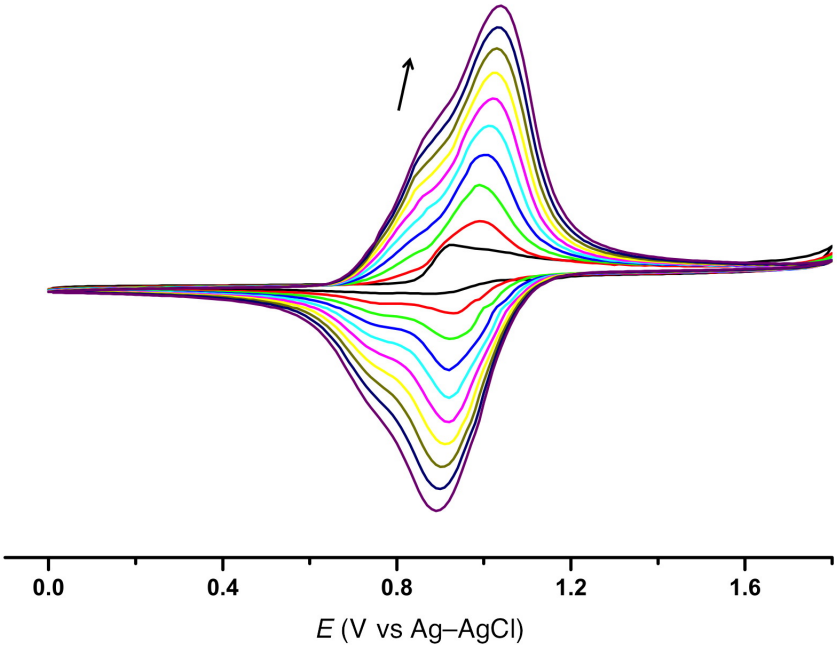

Figure S3. Cyclic voltammograms of complexes **3** (a) and **6** (b) recorded at 100 mV s^{-1} in DCM (0.1 M in $[N(C_4H_9\text{-}n)_4]PF_6$) with a glassy-carbon working electrode. The single-headed arrows indicate the increase in current with repeated cycles, due to the deposition of electroactive films.

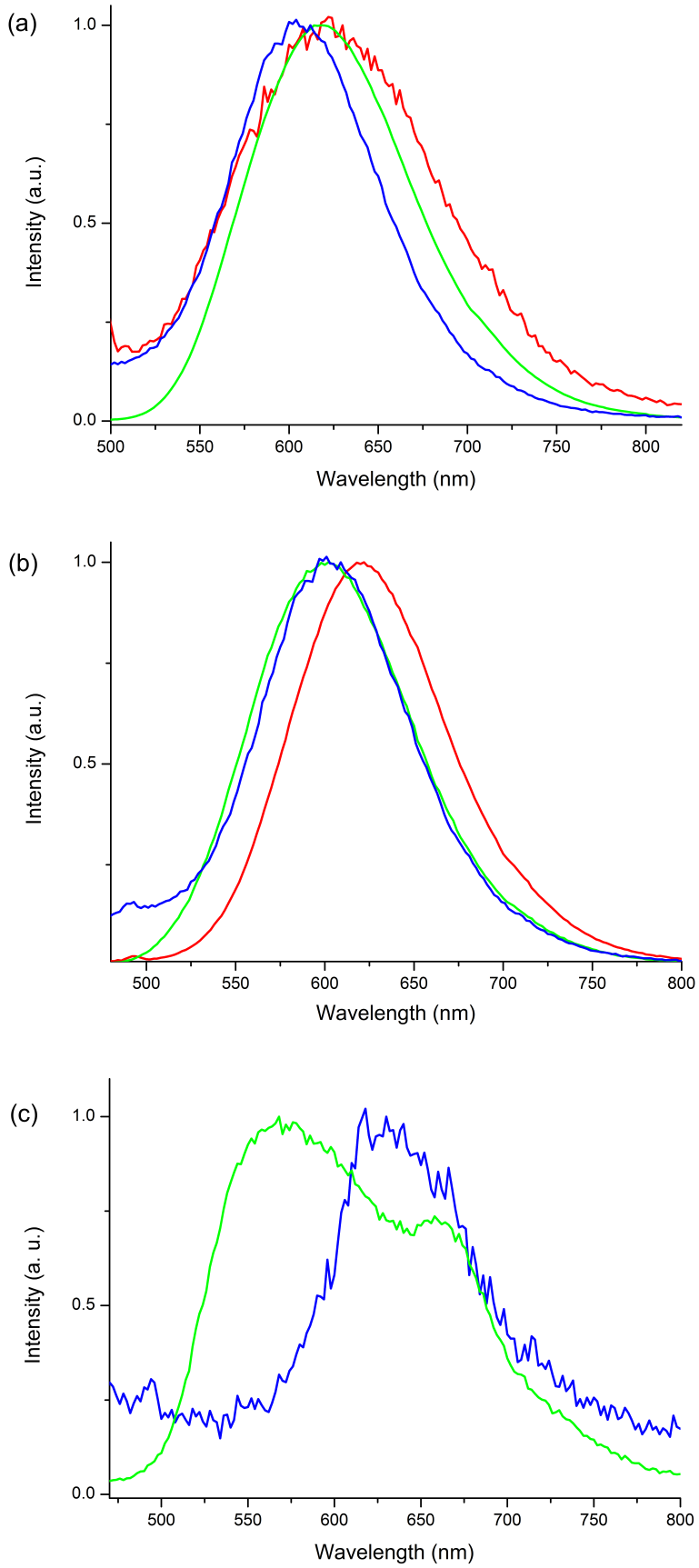

Figure S4. Emission spectra recorded in DCM at 293 K of: the $Zn^{II}Cl_2$ complexes **1** (blue), **2** (red) and **3** (green) (a); the $Zn^{II}OAc_2$ complexes **4** (blue), **5** (red) and **6** (green) (b); the $Re^{I}Cl(CO)_3$ complexes **7** (blue) and **9** (green) (c).

Table S1. Crystallographic Data and Refinement Details for $(Me_8Fcv)_2bpy$, 2, 4•$CHCl_3$ and 8•0.5$CHCl_3$

	$(Me_8Fcv)_2bpy$	**2**	**4**•$CHCl_3$	**8**•0.5$CHCl_3$
empirical formula	$C_{50}H_{60}Fe_2N_2$	$C_{50}H_{60}Cl_2Fe_2N_2Zn$	$C_{39}H_{35}Cl_3Fe_2N_2O_4Zn$	$C_{53.5}H_{60.5}Cl_{2.5}Fe_2N_2O_3Re$
fw	800.70	936.97	879.11	1166.06
cryst system	triclinic	monoclinic	triclinic	monoclinic
space group	$P\bar{1}$	$P2_1/c$	$P\bar{1}$	$P2_1/n$
a/Å	8.7387(9)	17.267(3)	9.8429(3)	15.8819(6)
b/Å	8.8209(8)	15.009(3)	12.5224(3)	14.5187(7)
c/Å	12.8954(15)	17.570(4)	15.4312(4)	24.1193(8)
α/deg	90.518(9)	90.00	84.808(2)	90.00
β/deg	95.357(9)	95.290(15)	73.656(2)	105.931(3)
γ/deg	92.272(8)	90.00	84.961(2)	90.00
U/Å^3	988.82(18)	4534.2(16)	1813.78(8)	5347.9(4)
Z	2	4	2	4
T/K	100(2)	100(2)	100(2)	200(2)
μ/mm^{-1}	6.157	7.027	9.494	10.090
cryst size/mm	0.1 × 0.05 × 0.02	0.05 × 0.02 × 0.01	0.1 × 0.05 × 0.05	0.11 × 0.09 × 0.06
cryst description	dark red needle	blue plate	red needle	green plate
reflns collected	8113	12349	21512	25805
independent reflns (R_{int})	3360 (0.1104)	4620 (0.2028)	6173 (0.0758)	9241 (0.1147)
θ_{max}/deg (completeness)	66.59 (96.1)	50.43 (97.4)	66.58 (96.2)	66.59 (97.7)
reflns with $I > 2\sigma(I)$	2529	2217	5028	6071
GOF on F^2	1.018	0.979	1.006	0.972
final $R1$, $wR2$ $[I > 2\sigma(I)]$	0.0718, 0.1645	0.0833, 0.1755	0.0618, 0.1636	0.0713, 0.1821
(all data)	0.0976, 0.1858	0.1952, 0.2383	0.0751, 0.1735	0.1086, 0.2018
peak and hole/eÅ^{-3}	0.68, –0.68	0.73, –0.62	0.99, –1.63	1.69, –1.23

Table S2. Luminescence Data for Complexes 1–9 in DCM

complex	λ_{em}, nm	
	λ_{exc} = 433 nm	λ_{exc} = 650 nm
1[a]	604	–[b]
2[a]	623	–[b]
3	619	tail to 800
4[c]	601	–[b]
5[c]	622	–[b]
6	602	tail to 760
7[a]	624	–[b]
8	–[b]	–[b]
9	569, 568sh	tail to 760

[a] Very weak emission. [b] None observed. [c] Weak emission.

(a)

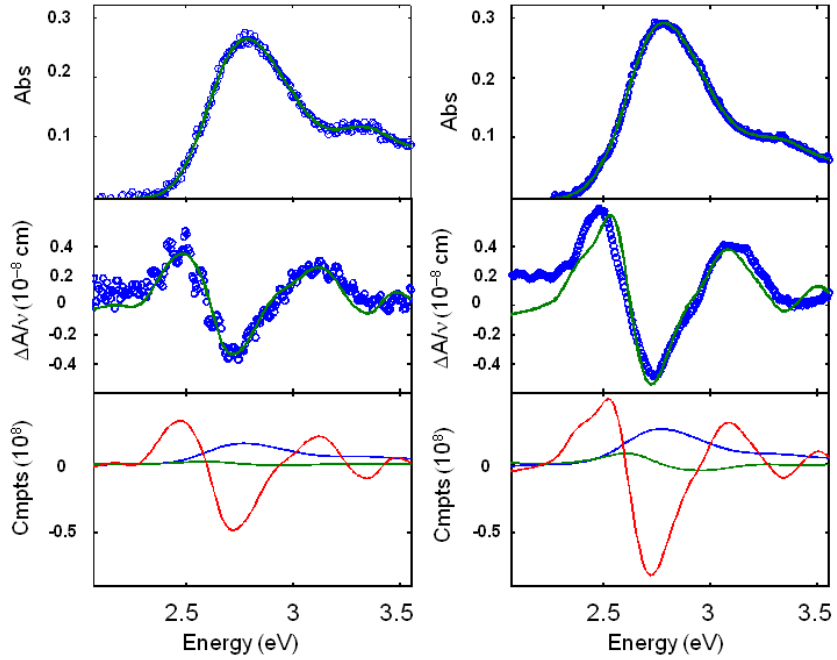

(b)

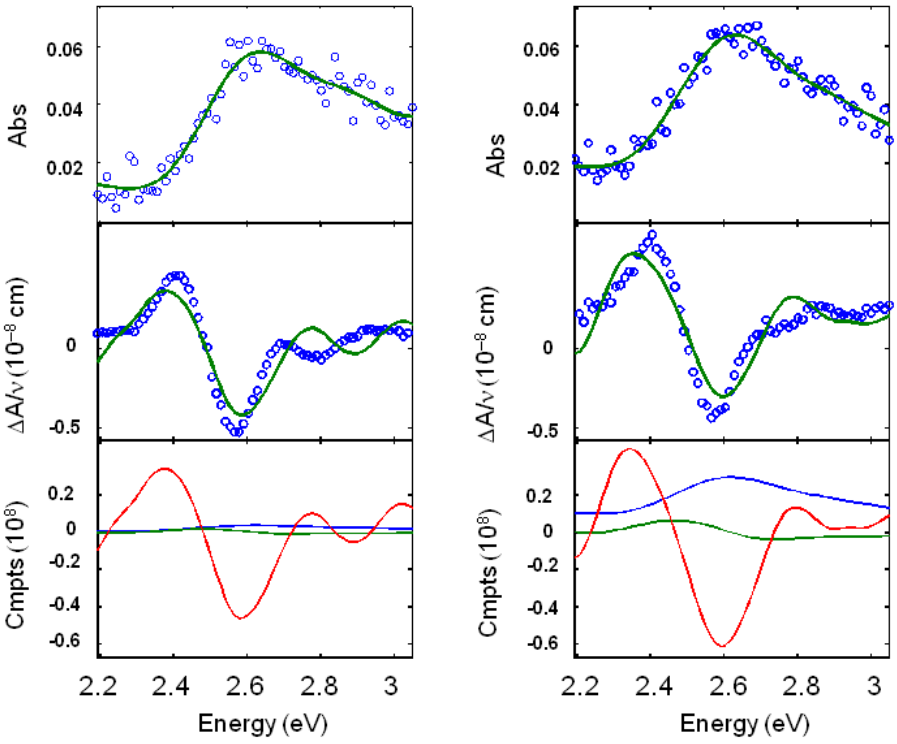

Figure S5. Spectra and calculated fits for the complexes **3** (a) and **9** (b) in butyronitrile at 77 K. Top panel: absorption spectrum; middle panel: electroabsorption spectrum, experimental (blue) and fits (green) according to the Liptay equation; bottom panel: contribution of 0th (blue), 1st (green) and 2nd (red) derivatives of the absorption spectrum to the calculated fits.

2. TD-DFT Calculated Contour Surface Diagrams

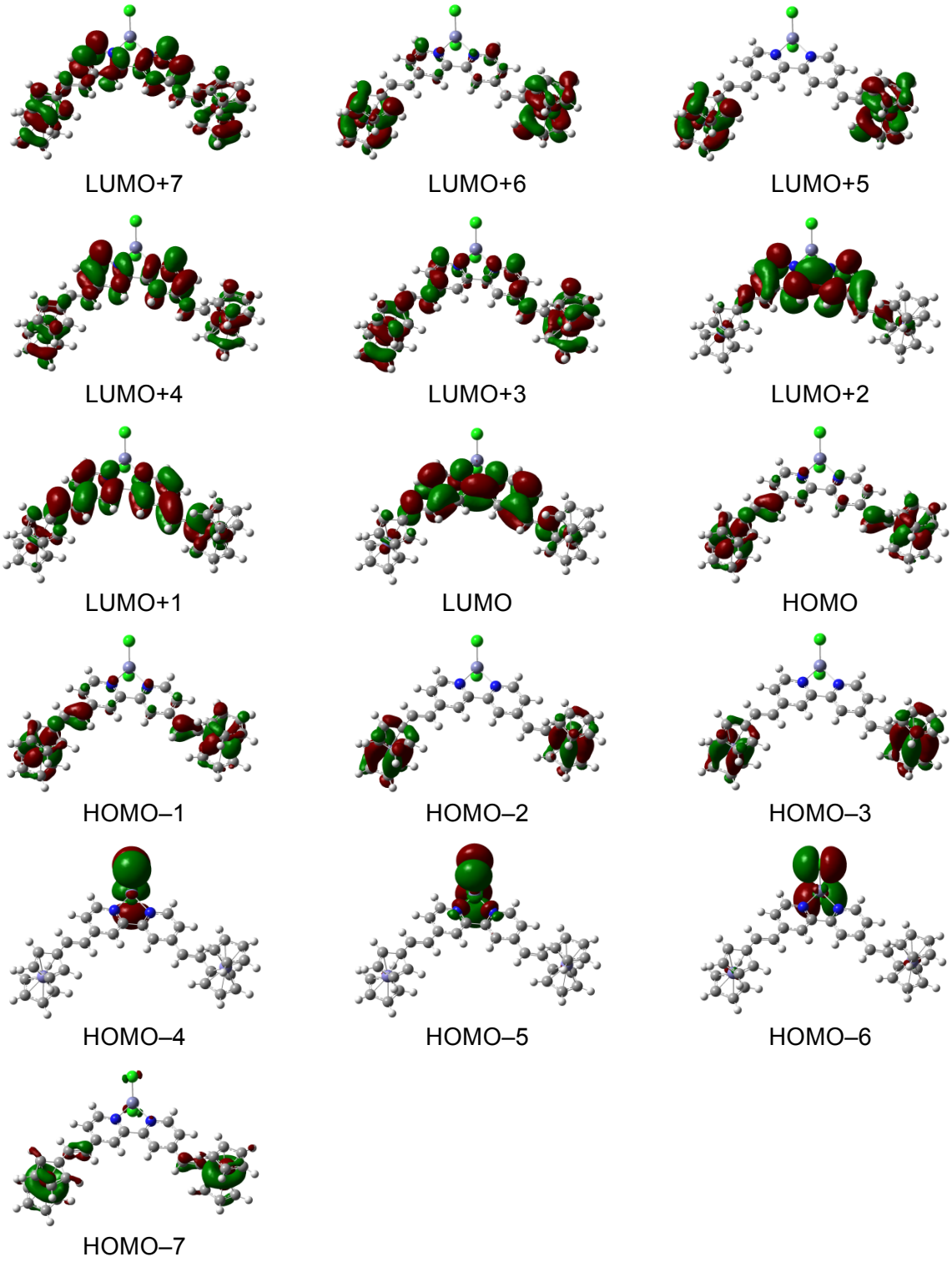

Figure S6. M06/Def2-TZVP/SVP/SVPP-derived contour surface diagrams of the frontier MOs for complex **1**.

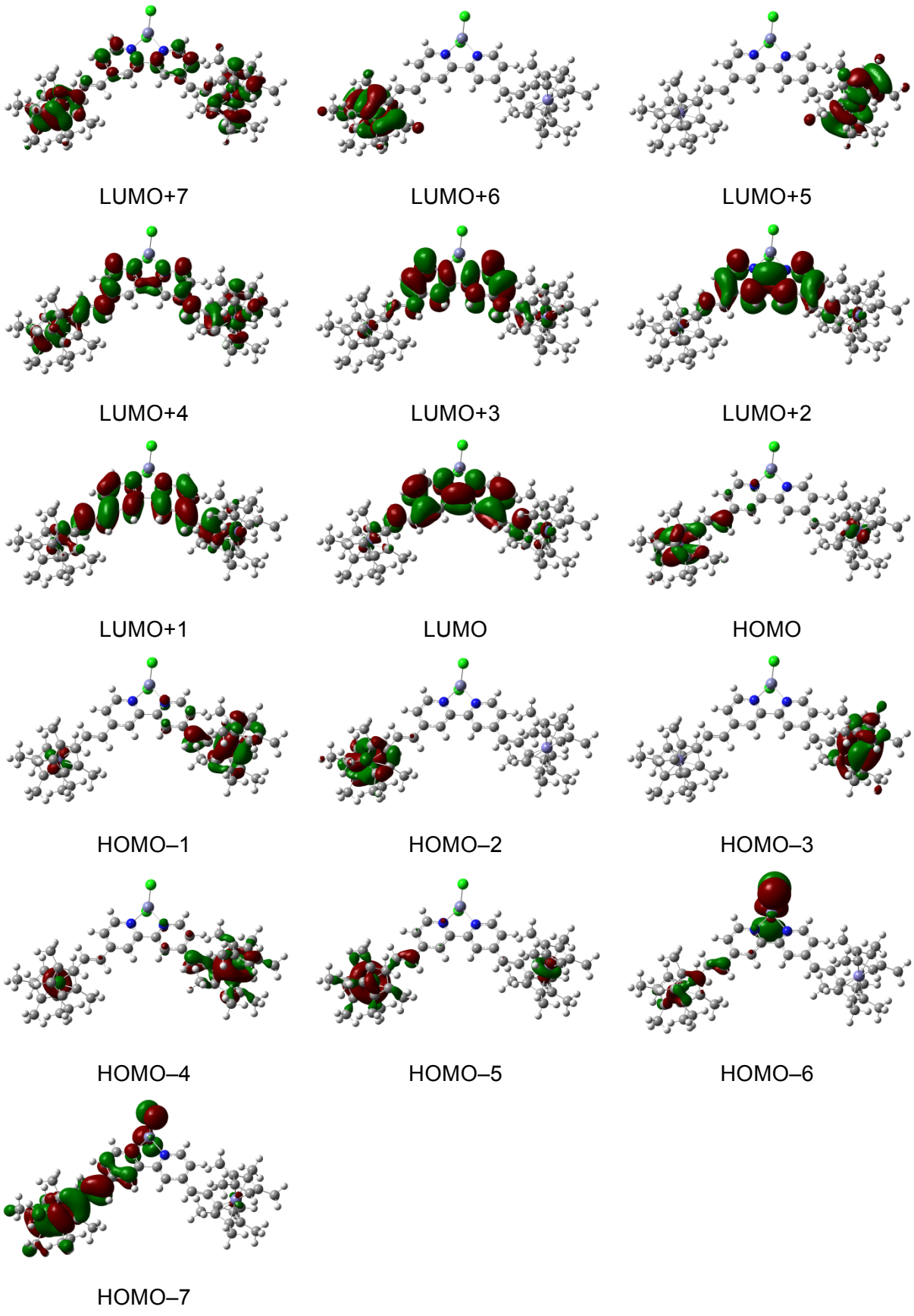

Figure S7. M06/Def2-TZVP/SVP/SVPP-derived contour surface diagrams of the frontier MOs for complex **2**.

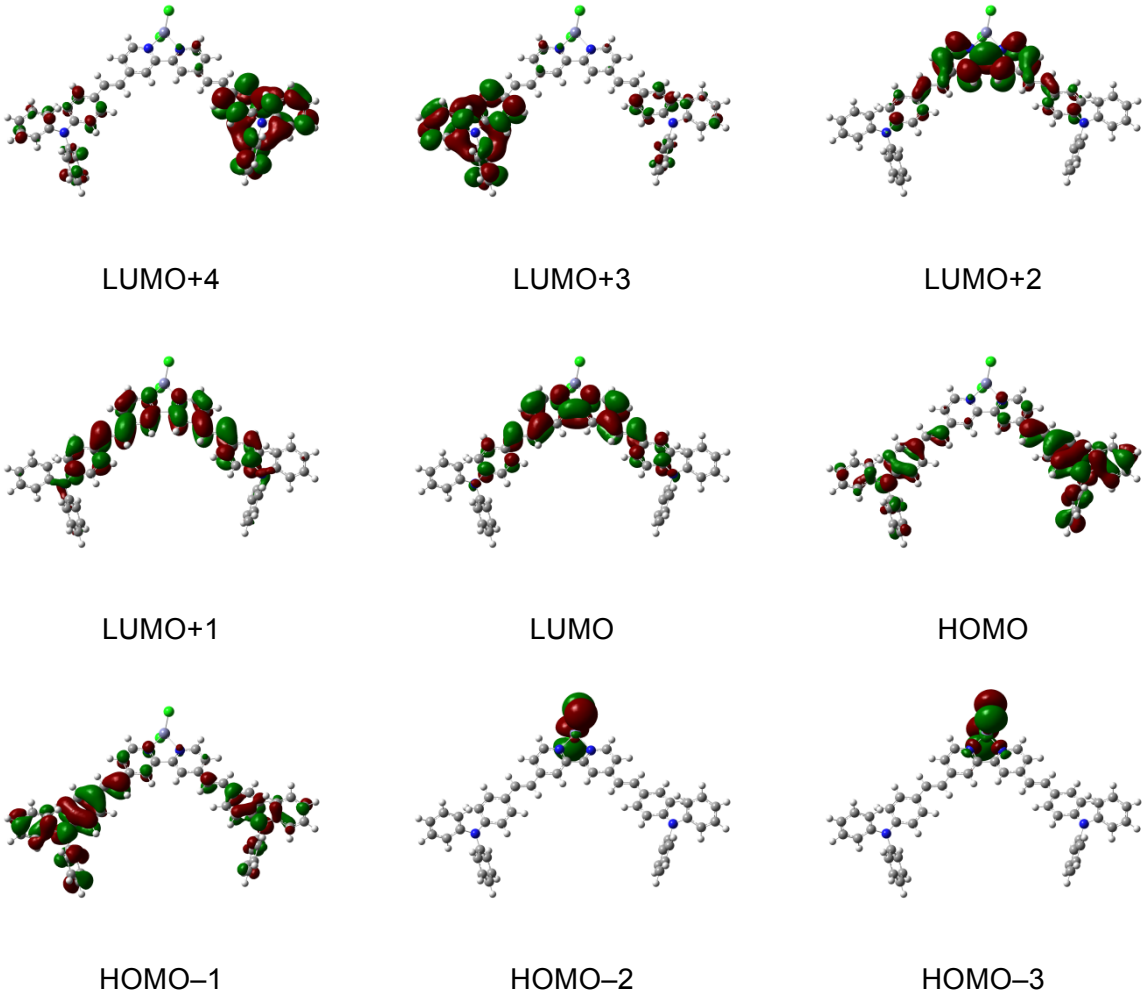

Figure S8. M06/Def2-TZVP/SVP/SVPP-derived contour surface diagrams of the frontier MOs for complex **3**.

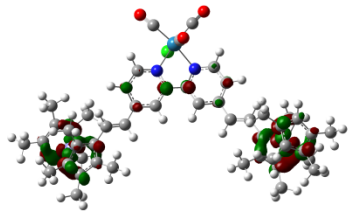

LUMO+9

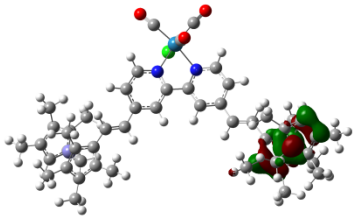

LUMO+8

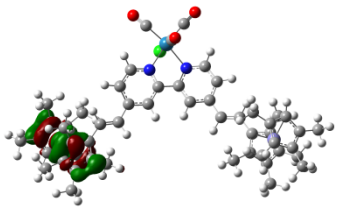

LUMO+7

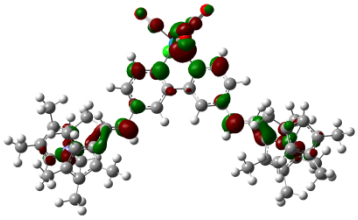

LUMO+6

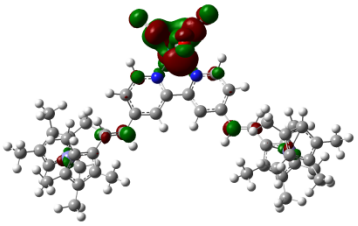

LUMO+5

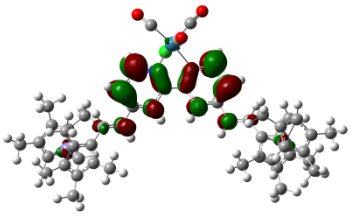

LUMO+4

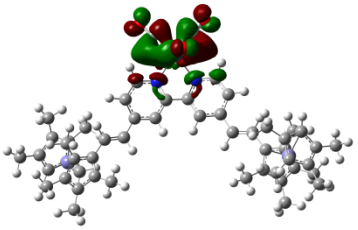

LUMO+3

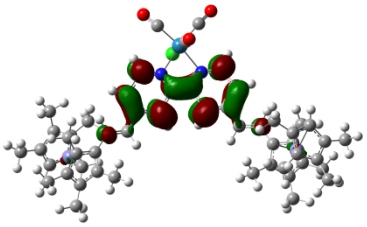

LUMO+2

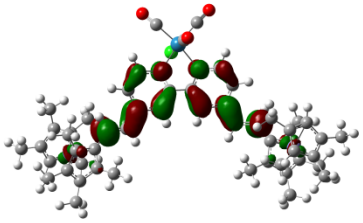

LUMO+1

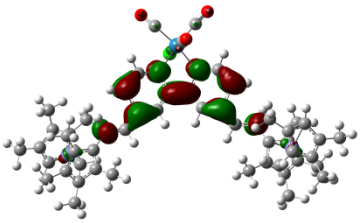

LUMO

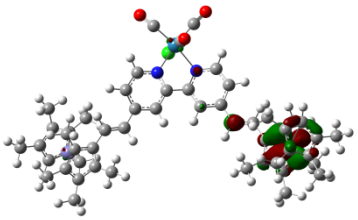

HOMO

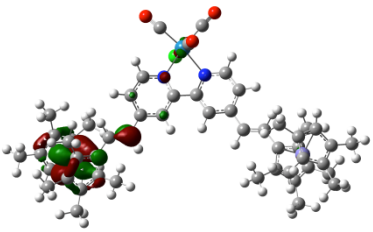

HOMO–1

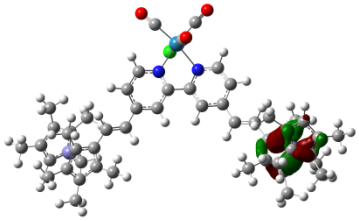

HOMO–2

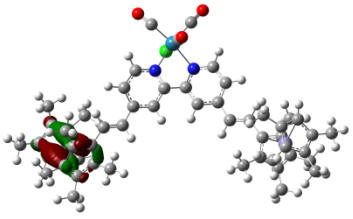

HOMO–3

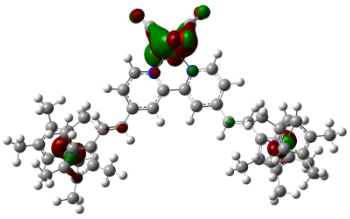

HOMO–4

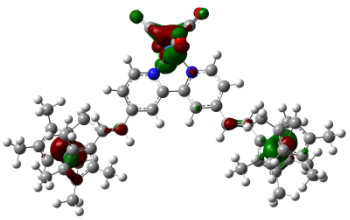

HOMO–5

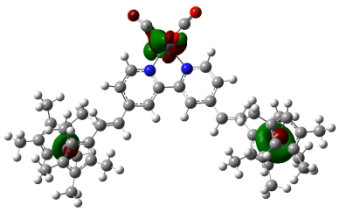

HOMO–6

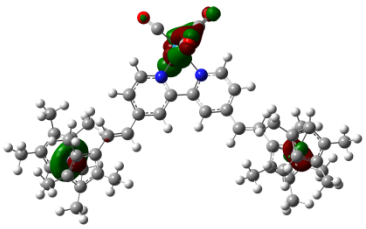

HOMO–7

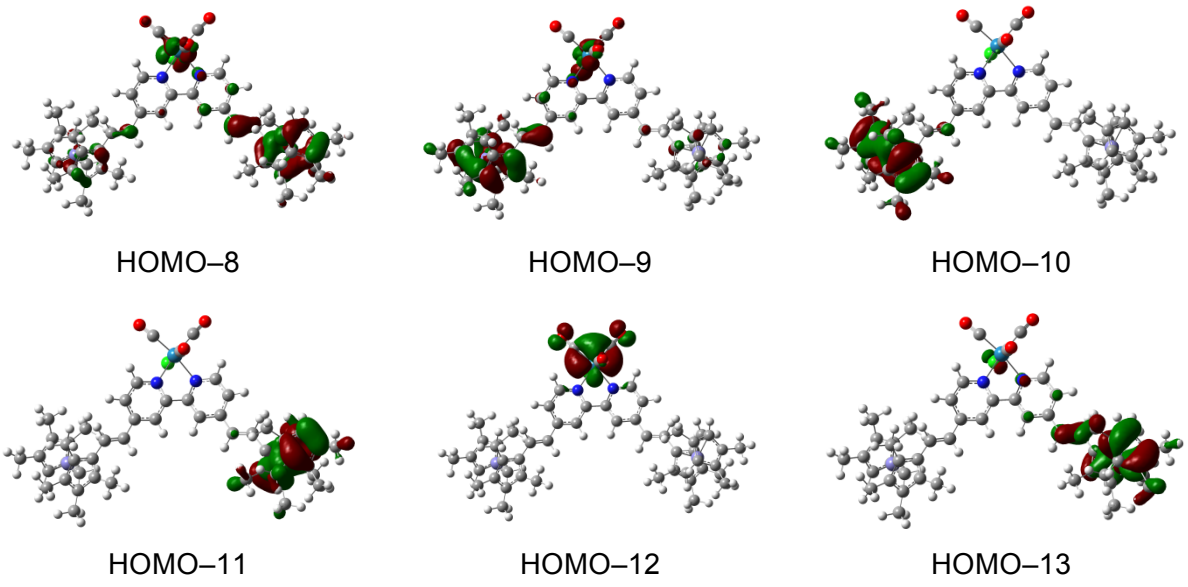

Figure S9. M06/Def2-TZVP/SVP/SVPP-derived contour surface diagrams of the frontier MOs for complex **8**.

3. TD-DFT Calculated UV–Vis data

Table S3. Selected TD-DFT-Calculated Data for the Complexes 1–3 and 8[a]

complex	ΔE (eV)	λ (nm)	f_{os}	μ_{12} (D)	major contributions (%)
1	1.97	628	0.02	0.74	H → L+4 (20); H–1 → L+7 (14); H → L (10); H–1 → L+1 (10); H–2 → L+6 (10)
	1.98	627	0.01	0.45	H–1 → L+4 (21); H → L+7 (15); H → L+1 (10); H–2 → L+5 (10); H–3 → L+6 (10)
	2.65	467	0.02	0.30	H–2 → L+6 (21); H–3 → L+5 (21); H → L (14)
	3.05	406	0.29	1.33	H → L (68)
	3.09	401	0.12	0.59	H–1 → L (71)
	3.41	363	0.12	0.90	H–4 → L (67)
	3.43	362	0.04	0.05	H–5 → L (71)
	3.55	350	0.38	1.74	H–6 → L (81)
	3.61	344	0.21	0.64	H–7 → L (83)
	3.66	339	0.12	1.41	H–1 → L+1 (41); H–3 → L+1 (27)
2	1.99	622	0.05	1.00	H–1 → L+7 (16); H–1 → L+1 (11)
	2.00	619	0.01	0.47	H → L+1 (10); H → L+7 (16)
	2.59	478	0.03	0.73	H–2 → L+6 (35); H → L (26)
	2.59	477	0.01	0.43	H–3 → L+5 (40); H–1 → L (26)
	2.89	430	0.26	1.92	H–1 → L (21); H → L (21); H–4 → L (10)
	2.92	424	0.06	0.89	H–1 → L (26); H → L (17)
	3.18	390	0.39	2.23	H–6 → L (34); H–4 → L (27)
	3.24	383	0.16	1.41	H–6 → L (50); H–4 → L (26)
	3.31	374	0.20	1.57	H–7 → L (80)
3	2.56	484	0.91	4.25	H → L (89)
	2.66	466	0.76	0.27	H–1 → L (93)
	3.13	396	0.38	3.40	H–1 → L+1 (83)
	3.14	395	0.48	0.31	H → L+1 (88)
	3.60	345	0.04	1.46	H → L+2 (85)
	3.61	343	0.03	0.16	H–1 → L+2 (86)
	3.79	327	0.34	2.48	H–2 → L (86)
	3.86	321	0.24	0.29	H–3 → L (91)
	3.91	317	0.02	2.49	H → L+3 (27); H → L+4 (25); H–1 → L+4 (23)
	3.91	317	0.04	2.25	H–1 → L+3 (33); H → L+4 (21); H–1 → L+4 (19); H → L+3 (13)

Table S3 (contd.)

complex	ΔE (eV)	λ (nm)	f_{os}	μ_{12} (D)	major contributions (%)
8	1.97	630	0.06	1.11	H–1 → L (15); H–1 → L+9 (14); H–1 → L+1 (11)
	1.97	628	0.02	0.65	H → L+9 (16); H → L (14); H → L+1 (10)
	2.53	491	0.12	1.36	H–6 → L (16); H–4 → L (10); H–3 → L+7 (10); H–2 → L+8 (13); H–1 → L (14); H → L (23)
	2.54	488	0.04	0.86	H–3 → L+7 (21); H–2 → L+8 (18); H–1 → L (25); H → L (14)
	2.65	469	0.04	0.78	H–6 → L+8 (11); H–5 → L (10); H–2 → L (32)
	2.65	469	0.05	0.88	H–5 → L (13); H–3 → L (25); H–2 → L (15)
	2.67	465	0.11	1.75	H–7 → L (10); H–5 → L (38); H–3 → L (18)
	2.82	439	0.15	1.47	H–6 → L (18); H–1 → L (14); H → L (17)
	3.10	400	0.31	2.02	H–12 → L (27); H–8 → L (28); H–4 → L (10)
	3.16	393	0.16	1.45	H–8 → L (42); H–6 → L (23)
	3.23	384	0.18	1.52	H–9 → L (78)

[a] Geometry optimizations and TD-DFT calculations used the M06 functional with the Def2-TZVP/SVP/SVPP mixed basis set, and a CPCM $CHCl_3$ solvent model was included for TD-DFT. Only the main transitions within each absorption band are included. H = HOMO, L = LUMO.